https://doi.org/10.5194/egusphere-2026-6668
Preprint. Discussion started: 12 November 2026
© Author(s) 2026. CC BY 4.0 License.

Size-resolved Spray-mediated CO_2 Flux: Sensitivity to Fall Speed Parameterization

Lucy Hendrickson, Penny Vlahos, Leonel Romero

Department of Marine Sciences, University of Connecticut, Groton CT, 06340, USA

Correspondence to: Lucy Hendrickson (lucy.hendrickson@uconn.edu)

Abstract. The magnitude of spray-driven air–sea fluxes is highly dependent on the residence time of the droplets in the atmosphere and the degree of evaporation they undergo. However, there is significant uncertainty in modeling spray fall speeds and therefore accurately estimating time aloft across the sea spray size spectrum. We compare the widely used terminal-velocity fall speed with a force-balance acceleration formulation that resolves acceleration over the droplet's full fall trajectory and assess the impact on modeled spray-driven CO_2 flux across the droplet size distribution over varying wind speed, sea state, and relative humidity (RH). Including force-balance acceleration reduces fall speed for all droplets with the greatest impact on droplets over 200 μm, with fall speed reductions up to 60 % for the largest drops. This change introduces competing effects at the individual droplet level, both increasing the size of droplets that undergo complete evaporation by 2–8 % under modeled conditions and also enhancing the CO_2 uptake of large cooling drops. However, the modest increase in the maximum evaporating droplet size of medium-sized droplets, which are numerous, has a substantially greater impact on the overall spray-driven CO_2 flux than the increase in CO_2 uptake by cooling spume droplets, which are comparatively rare. Moreover, the impact of fall-speed formulation is modulated by RH, with larger relative flux increases occurring at higher RH, where slower evaporation rates make droplets more sensitive to small changes in residence time. These combined effects drive an 18–26 % increase in net spray-driven CO_2 flux under modeled conditions. Fall-speed formulation is therefore an important source of uncertainty in spray-driven CO_2 flux estimates, particularly in the high-wind, developing-sea regime where spray dominates air–sea exchange.

Short Summary: When strong winds whip up sea spray, droplets can release carbon dioxide into the air, but how long the drops stay aloft is uncertain. We used a computer model to compare both a simple and a more realistic way of calculating how fast droplets fall. The realistic method lets larger droplets fall more slowly, raising spray-driven carbon dioxide exchange by 18 to 26 percent. Getting droplet fall speeds right matters for estimating how much carbon dioxide the ocean exchanges with the air in stormy seas.

https://doi.org/10.5194/egusphere-2026-6668
Preprint. Discussion started: 12 November 2026
© Author(s) 2026. CC BY 4.0 License.

1 Introduction

Sea spray droplets, generated by wind and breaking waves, influence a range of air–sea exchange processes. While aloft in the atmosphere, droplets undergo wet-bulb cooling and evaporation, driving heat, moisture, and gas transfer (Andreas, 1992; Andreas et al., 2017; Staniec et al., 2021). The extent of evaporation that droplets undergo determines their net flux contribution. Fully evaporating droplets also act as precursors to marine aerosol particles (Grythe et al., 2014). Consequently, the residence time (time aloft) of sea spray droplets is a fundamental control on spray-mediated fluxes and their broader atmospheric impact (Andreas, 1992). Droplet residence time is often estimated using the vertical distance between where the drop is generated to the surface (from the measured or modeled significant wave height) divided by the droplet fall speed (Andreas, 1990; Voermans et al., 2026; Barr et al., 2023). The droplet fall speed has historically been determined by the terminal velocity with or without drag-associated shape distortion of larger drops (Andreas, 1990; Beard, 1976), assuming droplets instantly reach terminal velocity and maintain that speed over their entire trajectory. Recent studies have compared the terminal velocity model to a force-balance acceleration model that assumes the droplet is stationary at its injection height and accelerates over its vertical trajectory, accounting for drag and associated droplet shape distortion (Voermans et al., 2026; van Boxel, 1998). The investigators found the latter approach more accurately matches observed sea spray droplet fall speed measured in lab experiments, especially for drops over 500 µm. Here, we assess the sensitivity of spray-mediated CO_2 flux to droplet fall speed formulation by comparing the widely used terminal-velocity approach with a trajectory-resolved force-balance formulation. We quantify the resulting changes in size-resolved droplet flux contributions across the droplet spectrum and examine how these changes propagate to net spray-mediated CO_2 flux estimates.

2 Methods

2.1 Comparison of fall speed formulations

Instantaneous-terminal fall speed $V_{f,term}$ is calculated in two ways, with and without accounting for droplet shape distortion. $V_{f,term}$ assuming a rigid sphere is calculated using the Stokes formula (Andreas, 1990), where ν_a is the kinematic viscosity of air

$$V_{f,term,Rigid} = \frac{2r^2 g}{9\,\nu_a\,[1+0.158\left(2r\frac{V_{f,Stokes}}{\nu_a}\right)^{\frac{2}{3}}]}\left(\frac{\rho_w}{\rho_a}-1\right). \quad (1)$$

$V_{f,term}$ accounting for droplet shape distortion is computed algebraically using the equations of Beard (1976), referred to hereafter as $V_{f,term,Dist}$.

https://doi.org/10.5194/egusphere-2026-6668
Preprint. Discussion started: 12 November 2026
© Author(s) 2026. CC BY 4.0 License.

$$V_{f,term,Dist} = \begin{cases} C_1 C_{sc}(2r^2)\ for\ 0.25\ \mu m \le r \le 15\ \mu m \\ \frac{\eta N_{Re,1}}{\rho_w(2r)}\ for\ 15\ \mu m \le r \le 500\ \mu m \\ \frac{\eta N_{Re,2}}{\rho_w(2r)}\ for\ 500\ \mu m \le r \le 3.5\ mm \end{cases} \quad (2)$$

The formulation for $V_{f,term}$ is broken into multiple equations across the droplet size range coefficients. The coefficients for the terms in Eq. (2) can be found in Table 1 of Beard (1976).

The force-balance acceleration fall speed formulation is calculated using the equations from van Boxel (1998) as implemented in Voermans et al. (2026),

$$\frac{4}{3}\pi r^3(\rho_w - \rho_a)g - C_D C_s \rho_a \pi r^2 v^2 = \frac{4}{3}\pi r^3 \rho_w a \quad (3)$$

where r is the droplet radius, ρ_a the air density, ρ_w the water density, g the gravitational acceleration, v is the instantaneous downward droplet velocity, a is the droplet acceleration, C_D the drag coefficient and C_s the shape factor, as calculated in van Boxel (1998). The two terms on the left-hand side represent the gravity and drag force, respectively (van Boxel, 1998; Voermans et al., 2026). Equation (3) is integrated along the droplet trajectory from release height H to the ocean surface. The residence time t_r is determined from the trajectory and converted to an effective settling velocity $V_{f,acc} = H/t_r$. Thus, the values shown for $V_{f,acc}$ represent trajectory-averaged settling velocities rather than an instantaneous droplet velocity.

Using this definition, Fig. 1 compares $V_{f,acc}$ calculated with and without accounting for shape distortion by including or excluding C_s the shape factor. In the comparison, we refer to the full $V_{f,acc}$ formula as the $V_{f,acc,Dist}$ fall speed, referring to the shape distortion, and the rigid-sphere $V_{f,acc}$ formulation as $V_{f,acc,Rigid}$. Including shape distortion in both $V_{f,term}$ and $V_{f,acc}$ models has no impact on droplets below 200 µm but there is a pronounced impact on larger radii when the spherical assumptions fail. For $V_{f,acc}$, where droplets over 200 µm do not achieve terminal velocity over 2.5 m, accounting for or disregarding shape distortion has little effect (Fig. 1a), but for $V_{f,term}$, the difference between parameterizations increases with droplet size up to 30 % (see $V_{f,term,Dist}$: $V_{f,term,Rigid}$ in Fig. 1b). The difference between $V_{f,term}$ and $V_{f,acc}$ ($V_{f,term,Dist}$: $V_{f,acc,Dist}$) ranges from 15 % to 60 %, increasing with droplet size and decreasing as fall height increases (Figs. 1b and 1d).

https://doi.org/10.5194/egusphere-2026-6668
Preprint. Discussion started: 12 November 2026
© Author(s) 2026. CC BY 4.0 License.

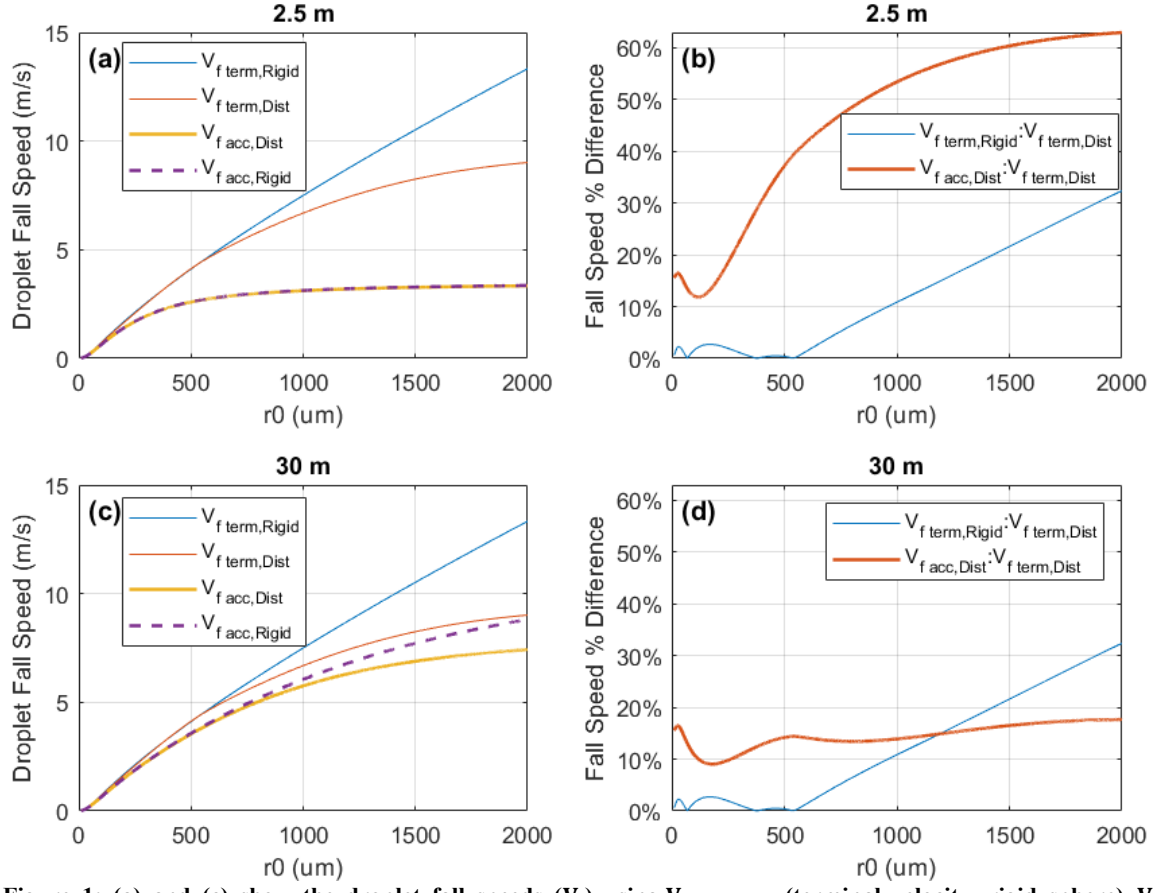


Figure 1: (a) and (c) show the droplet fall speeds (V_f) using $V_{f,term,Rigid}$ (terminal velocity, rigid sphere), $V_{f,term,Dist}$ (terminal velocity, shape distortion), $V_{f,acc,Rigid}$ (acceleration, rigid sphere), and $V_{f,acc,Dist}$ (acceleration, shape distortion) fall speeds over droplet sizes of initial radius r_0. (b) and (d) quantify the ratio of the fall speed formulations. (a) and (b) have a fall height of 2.5 m, (c) and (d) have a fall height of 30 m.

Two fall heights are modeled in Fig. 1: a height of 2.5 m, shown in the top row, which is used here as an example of significant wave height in rough seas for winds over 15 m s^{-1}, and 30 m, shown in the lower row, an exaggerated upper bound used to illustrate the limiting case in which droplets have sufficient distance to approach terminal velocity. Consequently, the influence of the fall height on $V_{f,acc}$, is substantially reduced in the 30 m case, although such wave heights are generally unrealistic under normal ocean conditions. Increasing the wave height and therefore the injection height leads to a smaller discrepancy between the $V_{f,term}$ and $V_{f,acc}$ models. When the droplet fall height is extended to 30 m (Fig. 1c), more droplets reach terminal velocity in the $V_{f,acc}$ model. At higher wind speeds and lower injection heights the difference between the rigid droplet formulas and the shape-distortion assumptions becomes increasingly significant. The $V_{f,term}$ ratio ($V_{f,term,Dist}$: $V_{f,term,Rigid}$) does not change since neither parameterization is sensitive to fall height.

Including the force balance acceleration decreases droplet fall speed relative to terminal velocity and therefore increases residence time and time for both evaporation and outgassing. For a 2.5 m fall height, a significant reduction in fall speed is

https://doi.org/10.5194/egusphere-2026-6668
Preprint. Discussion started: 12 November 2026
© Author(s) 2026. CC BY 4.0 License.

introduced for droplets over 200 µm (Fig. 1a). Instantaneous terminal fall speed parameterizations are insensitive to fall distance, but force-balance-acceleration parameterizations are affected by fall height, especially for large drops that experience additional drag due to shape distortion and which may never reach terminal velocity for relatively low injection heights. In order to apply these terminal/acceleration paradigm differences to sea-spray driven CO_2 flux, only the more realistic, nonrigid formulations for $V_{f,term}$ ($V_{f,term,Dist}$) and $V_{f,acc}$ ($V_{f,acc,Dist}$) are used for the subsequent analyses.

2.2 Spray-driven CO_2 flux model

Spray-driven CO_2 flux is modeled following Hendrickson et al. (2026). ϕ is the individual droplet CO_2 flux contribution

$$\phi(r_0, \tau_f) = \int \left(CO_{2gen}(pH(r,t), DIC(r,t)) - CO_{2atm}\right) dt. \quad (4)$$

It is the integral, over the droplet's time aloft, of the difference between the ambient pCO_2 and the droplet's internal pCO_2 at each timestep. This pCO_2 difference is generated within the droplet by carbonate chemistry reactions dependent on the droplet's dissolved inorganic carbon (DIC) and pH, which change as it evaporates. At each timestep, the DIC is also adjusted to account for carbon lost through outgassing (Eq. (4)).

A droplet goes through two subsequent phases of cooling and evaporation. ϕ can give a net CO_2 outgassing or uptake for a droplet, depending on its degree of cooling and evaporation, which are functions of its size and residence time as well as relative humidity. Large drops with brief residence times cool and take up atmospheric CO_2, while smaller droplets with longer residence times evaporate significantly.

Significant evaporation results in a pH drop and salinity spike. The model replicates the measured spray pH range of 2-5 (Keene et al., 1998, 2002; Fridlind and Jacobson, 2000; Pszenny et al., 2004; Angle et al., 2021). Evaporation is used in the model as a metric of droplet chemical evolution rather than a driver of acidification, since volumetric concentration scales alkalinity as well. The observed acidification of spray is caused by the uptake of strong atmospheric acids including HNO_3, H_2SO_4, and HCl, with droplet pH then buffered by HSO_4^-/SO_4^{2-} equilibria and HCl partitioning (Keene et al., 1998, 2002). This process causes chemical conversion of dissolved carbonate and bicarbonate into CO_2 which is then forced out of the drop by increasing partial pressure through chemical production of CO_2 and decreasing solubility (Weiss, 1974). This is a unique feature of the carbonate reaction cascade in seawater, resulting in evaporating spray drops evading far more CO_2 gas relative to a nonreactive gas, while droplets that cool, but do not evaporate, take up CO_2, contributing a competing net effect on spray-driven CO_2 flux (Hendrickson et al., 2024, 2025). The direction and magnitude of net spray-driven flux (F_{spray}) is therefore highly sensitive to the droplet size distribution, total volume of spray production, and the residence time of each droplet size class.

The total spray-driven contribution to CO_2 flux F_{spray} (Eq. (5)) is the number of droplets produced at each size class (N, # of droplets m^{-2} s^{-1} μm^{-1}, calculated using the sea spray generation function published in Barr et al., 2023) times ϕ, the net CO_2 flux driven by individual droplets of that size class integrated over the droplet size distribution

https://doi.org/10.5194/egusphere-2026-6668
Preprint. Discussion started: 12 November 2026
© Author(s) 2026. CC BY 4.0 License.

$$F_{spray} = \int N\left(r_0, \tau_f, U_{10}, F_P, H_S, u_*, \epsilon, W, S\right)\phi\left(r_0, \tau_f\right)dr_0 \quad (5)$$

where the wind speed U_{10}, peak frequency F_P, significant wave height H_S, friction velocity u_*, energy dissipation ϵ, whitecap coverage W, and mean squared wave slope S were modeled using idealized WaveWatch3 (WW3) wave solutions (Romero, 2019; Hendrickson et al., 2026; Barr et al., 2023).

The difference between spray-driven flux calculated using the two residence time formulations is shown in Eq. (6):

$$\Delta F_{spray} = F_{spray}(\tau_{acc}) - F_{spray}(\tau_{term}) \quad (6)$$

In the following sections, we quantify the effects of changing fall speed on F_{spray} relative to the effects of relative humidity (RH) and sea state.

3 Results

3.1 Individual droplet CO_2 flux

In this analysis, we model scenarios where $T_{air} = T_{water}$ at 20 °C at 80 % and 90 % RH, which means that all drops experience wet bulb cooling upon injection to the atmosphere before evaporation. Residence time limits droplet progression through the sequential stages of thermal equilibration and evaporation. Time to thermal equilibration is similar for both 80 % and 90 % RH, while the time to fully evaporate is longer for higher humidity.

Across the droplet size spectrum, there is a size class below which droplets experience net evaporation and ϕ is positive (net CO_2 efflux per drop) and above which droplets initially cool and approach thermal equilibrium, but do not evaporate significantly, and ϕ is negative (net CO_2 uptake per drop). This transitional droplet size is denoted by r_0^*, the largest droplet size at which ϕ is positive. r_0^* increases with lower RH and is consistently larger for $V_{f,acc}$ (Fig. 2, solid black lines) relative to $V_{f,term}$ (Fig. 2, dashed black lines). Red shading marks droplet radii up to r_{peak}, which is the maximum droplet size that experiences full evaporation, and blue shading marks droplet radii r_{therm} that do not complete thermal equilibration (extended residence time enhances the amount of CO_2 they take up as they progress to thermal equilibrium). The unshaded region in the center marks the radii $r_{evap,part}$ where droplets complete thermal equilibrium and experience partial evaporation. r_0^* must be located in this region. The droplet size range between r_0^* and r_{therm} is therefore reduced as r_0^* increases. Droplets in this range complete thermal equilibration and experience very little evaporation, so that their net contribution is uptake of CO_2. These transitional radii shift with environmental parameters, including air–sea temperature difference, relative humidity, wind speed, and sea state, since these factors affect the speed and degree of evaporation that droplets experience aloft.

Under the modeled conditions, all droplets under 40 µm at 80 % RH, or 30 µm at 90 % RH, are aloft long enough to completely evaporate and expel all of their dissolved inorganic carbon as CO_2. Droplets between 40–300 µm or 30–300 µm (at 80 and 90 % RH respectively), are aloft long enough to achieve thermal equilibration and partial evaporation. r_{therm}

https://doi.org/10.5194/egusphere-2026-6668
Preprint. Discussion started: 12 November 2026
© Author(s) 2026. CC BY 4.0 License.

begins at 300 µm in both cases, since the modeled 10 % RH difference has minimal effects on the time to thermal equilibration in these conditions. Droplets larger than 300 µm do not reach thermal equilibration. These drops may experience moderate CO_2 uptake while aloft due to wet bulb cooling of the outer water film. Note these results are based on a very specific scenario of zero air water temperature change to isolate the components of interest. Under different temperature gradients, sea states, and relative humidities there will be a shift in these three sea spray size classes.

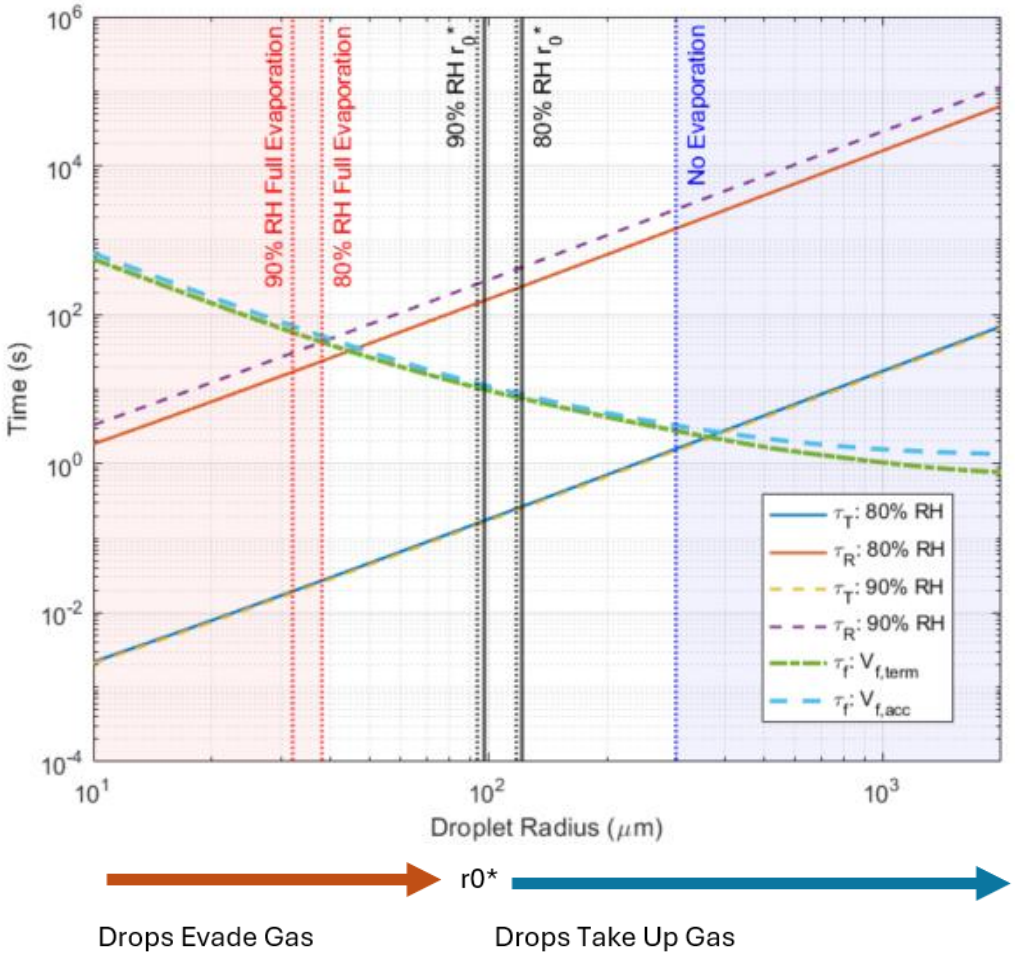


Figure 2: Residence times using $V_{f,term}$ and $V_{f,acc}$ compared to the time to thermal equilibrium and full evaporation across the droplet size range. r_0^* for both fall speeds (broken black lines for $V_{f,term}$ and solid black lines for $V_{f,acc}$) at each RH (at 15 m s^{-1} wind and 3.7 m waves) mark the droplet size where, under these conditions, droplet evaporation is limited and no longer drives CO_2 efflux. Red shading marks droplet radii that experience full evaporation and blue shading marks droplet radii that do not complete thermal equilibration. The unshaded region in the center marks the radii where droplets complete thermal equilibrium and experience partial evaporation.

r_{peak} and r_0^* both increase slightly for $V_{f,acc}$ relative to $V_{f,term}$. The additional evaporation experienced by droplets in this intermediate range, 40–200 µm under these conditions, increases their CO_2 efflux contributions, as shown in Fig. 3. In this size range, droplets complete the cooling phase, during which they take up CO_2, and subsequently experience partial

https://doi.org/10.5194/egusphere-2026-6668
Preprint. Discussion started: 12 November 2026
© Author(s) 2026. CC BY 4.0 License.

evaporation, during which they produce and evade additional CO_2. As droplet size increases, the degree of evaporation decreases until the directionality of their net CO_2 flux changes at r_0^*. Here, extending residence time increases the degree of evaporation, causing r_0^* to shift to larger droplet sizes. Since droplets smaller than r_{peak} for $V_{f,term}$ already fully evaporate, increasing their residence time has no effect. The increase in r_{peak} and r_0^* quantifies the additional CO_2 efflux driven by a greater degree of evaporation through extended residence time. In contrast, r_{therm} does not shift, indicating that the size range at which very large spume droplets fail to reach thermal equilibration is less sensitive to changes in residence time.

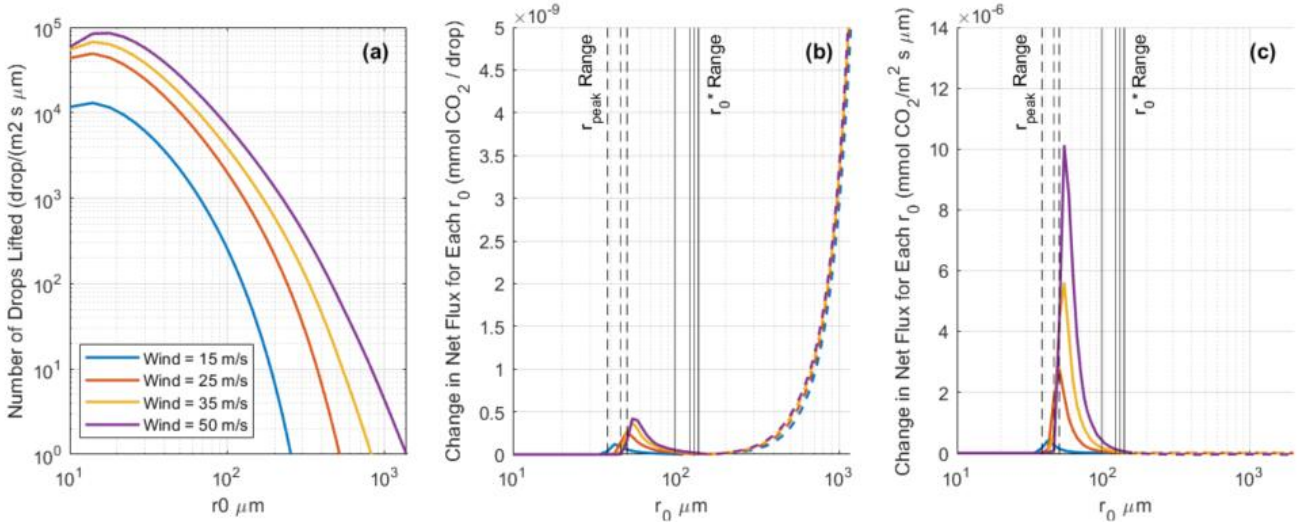


Figure 3: At 80 % RH: (a) the size-resolved droplet production $N(r_0)$, (b) change in per-drop CO_2 flux $\Delta\phi(r_0)$ and (c) change in per-drop CO_2 flux $\Delta\phi(r_0)\,N(r_0)$ produced. Solid lines in (b) and (c) indicate CO_2 efflux and broken lines indicate CO_2 uptake. r_{peak} marks the largest radii that experience full evaporation using $V_{f,term}$, and r_0^* marks the largest radii that experience net CO_2 efflux using $V_{f,acc}$. These two transitional radii bound the droplet size range where efflux is increased. Note that r_{peak} for $V_{f,acc}$ is slightly larger than r_{peak} for $V_{f,term}$.

For droplets larger than r_0^*, CO_2 uptake per droplet increases with size, accelerating once drops are larger than r_{therm} and no longer experience significant evaporation. For droplets in this size range, increasing residence time increases their net uptake of CO_2. Recalling Fig. 1b, the ratio of $V_{f,acc}$: $V_{f,term}$ shows that replacing $V_{f,term}$ with $V_{f,acc}$ has a stronger effect on large drops that have more drag due to shape distortion and take longer to accelerate to terminal velocity. Since the difference between $V_{f,term}$ and $V_{f,acc}$ is greatest in this size range, the magnitude of this change is also much greater than the magnitude of CO_2 efflux enhancement for smaller droplets.

However, the size distribution of spray $N(r_0)$ determines the net effect of each droplet size class. Figure 3a shows that the production of small droplets significantly exceeds larger ones, although droplet size ratios change with increasing winds as production of large droplets increases. Figure 3c shows the change in individual droplet CO_2 flux, ϕ, replacing $V_{f,term}$ with $V_{f,acc}$, scaled by $N(r_0)$, the number of spray droplets of each size class. While large droplets over 200 μm may have a disproportionate impact on an individual level, their low abundance means that their net effect is low.

https://doi.org/10.5194/egusphere-2026-6668
Preprint. Discussion started: 12 November 2026
© Author(s) 2026. CC BY 4.0 License.

Due to the number of droplets produced between 40–200 µm, however, a slight shift in r_0^* can drive a significant change in F_{spray}. r_0^* values for 80 % RH (Fig. 4a) range from 60–170 µm, depending on wind and sea state, while the r_0^* range for 90 % RH (Fig. 4b) is 45–135 µm. Across both RH scenarios however, r_0^* for each sea state or windspeed is always greater for $V_{f,acc}$ than it is for $V_{f,term}$.

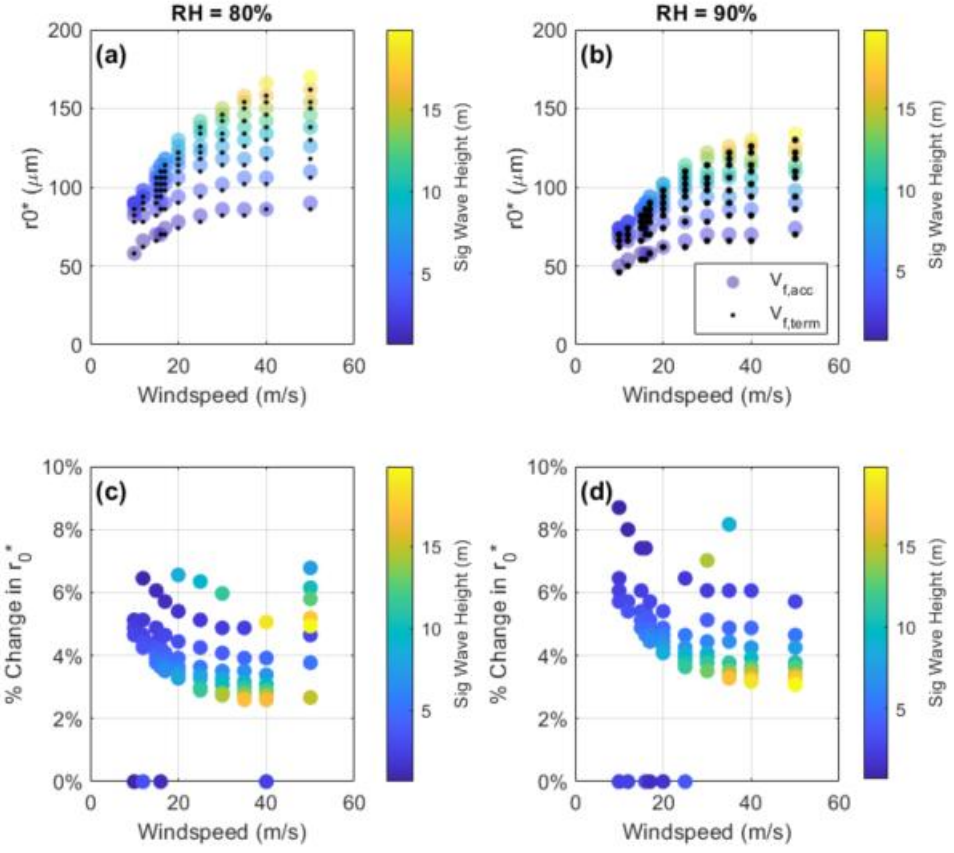


Figure 4: (a) and (b) show the change in r_0^* for 80 % and 90 % RH. Black markers are spray flux results using $V_{f,term,Dist}$ ($V_{f,term}$), $V_{f,acc,Dist}$ ($V_{f,acc}$) spray flux results are shown in colored markers shaded by significant wave height. (c) and (d) show the percent change in r_0^* for results calculated using $V_{f,acc,Dist}$ and $V_{f,term,Dist}$ fallspeeds at 80 % RH and 90 % RH, respectively.

Across both fallspeed formulations, r_0^* increases with increasing wind speed and wave height (Figs. 4a and 4b), which also extend residence time. Note r_0^* changes significantly at each wind speed based on sea state. Although r_0^* values are larger at 80 % than 90 % RH, the change in r_0^* due to fallspeed formulation is larger for 90 % RH than for 80 % RH, consistent with the net CO_2 flux results in Fig. 5.

The percent change in r_0^* at any given set of wave height conditions is less than 10 % in all cases, showing that even a small change in residence time and the size of droplets that experience net evaporation can have a strong effect on net spray-driven CO_2 flux if the change is within the range of droplet sizes that have the highest production rates.

https://doi.org/10.5194/egusphere-2026-6668
Preprint. Discussion started: 12 November 2026
© Author(s) 2026. CC BY 4.0 License.

3.2 Net spray-driven CO_2 flux

The net spray-driven CO_2 flux (F_{spray}) across wind speeds and sea states for idealized wave data from WW3 is shown in Fig. 5 and compared to interfacial flux (W14) and bubble-enhanced flux (DM18) models (Romero, 2019; Wanninkhof, 2014; Deike and Melville, 2018). Figure 5a shows model results at 80 % RH, and Fig. 5b shows results at 90 % RH. Modeled spray-driven CO_2 flux is consistently higher in magnitude at 80 % RH than at 90 % RH, for both fall speed formulations due to increased evaporation rate. Figures 5c and 5d quantify the percent difference in F_{spray} at each windspeed and sea state after replacing $V_{f,term}$ with $V_{f,acc}$ for each RH. Spray-driven CO_2 efflux modeled using $V_{f,acc}$ is consistently 18–26 % higher than results using $V_{f,term}$, depending on RH and sea state.

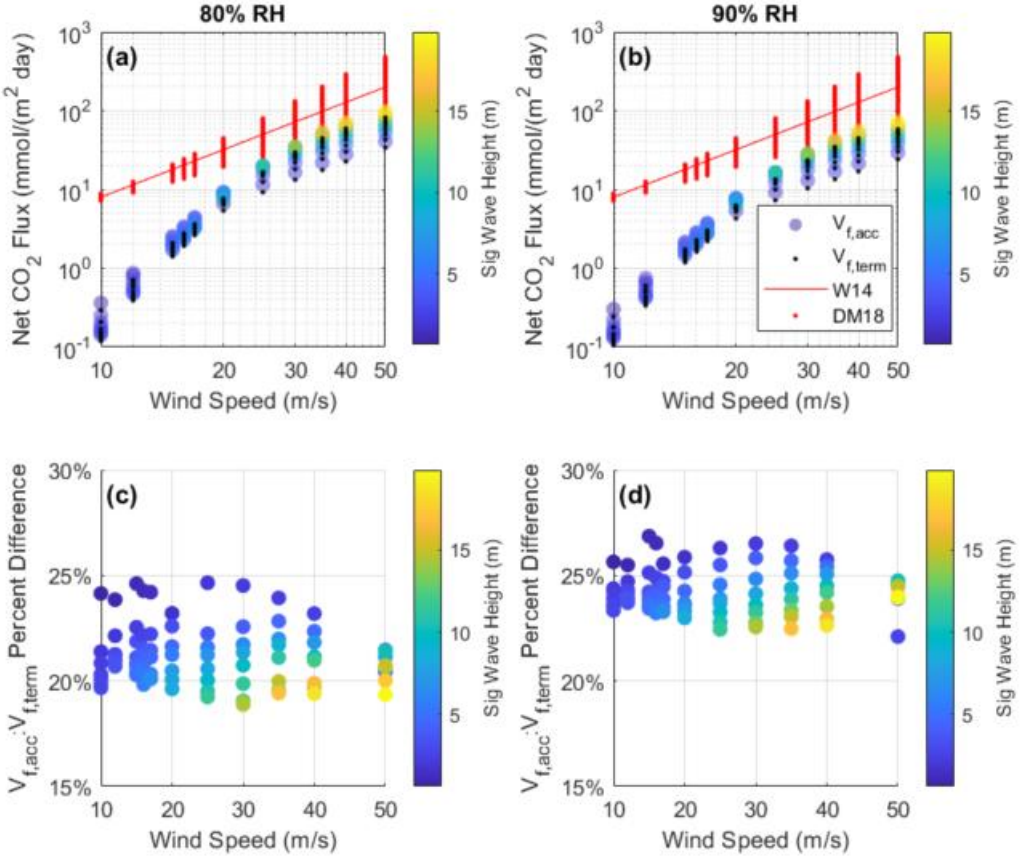


Figure 5: (a) and (b) show net CO_2 flux for increasing wind and varying sea states for 80 % and 90 % relative humidity, respectively. $V_{f,acc}$ spray flux results are shown in colored markers shaded by significant wave height. Black markers are spray flux results using $V_{f,term}$. The red line is interfacial flux (W14), red bars are the bubble-enhanced flux range across sea states (DM18). (c) and (d) show the percent difference between results calculated using $V_{f,acc}$ and $V_{f,term}$ fallspeeds at 80 % RH and 90 % RH.

The percent change at 90 % RH (~25 %) is greater than at 80 % RH (~20 %) even though absolute flux at 90 % RH remains lower than absolute flux at 80 % RH for both fallspeed formulations. In other words, fall speed formulation is more

https://doi.org/10.5194/egusphere-2026-6668
Preprint. Discussion started: 12 November 2026
© Author(s) 2026. CC BY 4.0 License.

significant when evaporation is slower and the magnitude of net spray CO_2 flux is lower. Similarly, the percent change in F_{spray} between $V_{f,term}$ and $V_{f,acc}$ formulations is greatest at lower wind speeds and low wave heights. $V_{f,term}$ and $V_{f,acc}$ F_{spray} results converge under stronger winds and more developed sea states, since higher sea states reduce the discrepancy between the two fall speed formulations (Fig. 1).

4 Discussion and Conclusions

Residence time significantly affects the net impact of a generated droplet population and fall speed formulation affects residence time. Replacing $V_{f,term}$ with $V_{f,acc}$ extends residence time, enhancing spray-driven CO_2 fluxes by shifting the size of droplets that completely evaporate and the degree of evaporation and range for intermediate sized droplets whose partially evaporation drives net CO_2 efflux. The intermediate size range for droplets was 30–50 µm to 100–200 µm depending on wind speed, sea state, and relative humidity. r_{peak} and r_0^* shifted up to 20 % and up to 8 % when $V_{f,acc}$ was used. These modest shifts led to an increase in spray-driven CO_2 efflux (F_{spray}) by around 18–26 %, for windspeeds between 15 and 50 m s^{-1}. At 80 % RH, droplets evaporate rapidly and most of the flux-contributing size range is already saturated by the shorter $V_{f,term}$, so a slight residence time extension with $V_{f,acc}$ adds comparatively little net CO_2 flux, while the effect is slightly larger for 90 % RH.

The 18–26 % change in net spray-driven CO_2 flux by replacing $V_{f,term}$ with $V_{f,acc}$ shown here is specific to the modeled conditions, and is not a universal correction factor. There is no simple scaling between changes in droplet residence time and changes in net spray-driven CO_2 flux. Increased residence time does not uniformly enhance CO_2 efflux across the droplet size spectrum. $V_{f,acc}$ does increase evaporation and efflux both by increasing the radius of complete evaporation and by increasing the degree of evaporation for intermediate droplets, but it also increases cooling and gas uptake for droplets over 200 µm, and the magnitude of the latter is larger than that of the former. The relative significance of these changes to an individual droplet's flux contribution is determined by the competition between these droplet populations, and their relative production. Changes to the net spray-driven CO_2 flux, F_{spray}, are the result of these nonlinear, directionally conflicting processes, dependent on spray size distribution and total magnitude.

This study isolates vertical settling trajectories but does not include turbulent advection, wave-coherent airflow, or horizontal droplet transport. This ballistic approach is common in sea spray modeling, neglecting three-dimensional transport for the sake of reduced computational load. The consequences of this simplification for residence time are wind-regime dependent. Lagrangian stochastic simulations resolving three-dimensional turbulent transport (Mueller and Veron, 2014) show that free-fall estimates based on wave height and terminal velocity depart from directly simulated residence times by a factor of 0.5–2. The direction of the bias changes across wind speed: at low-to-moderate winds, free-fall estimates predict longer residence times than the turbulence-resolving model for all but the largest, ejection-velocity-dominated drops, while above roughly 30 m s^{-1} turbulent transport instead extends residence time beyond the free-fall prediction as settling becomes subordinate to

https://doi.org/10.5194/egusphere-2026-6668
Preprint. Discussion started: 12 November 2026
© Author(s) 2026. CC BY 4.0 License.

vertical velocity fluctuations. Because our highest-wind cases (>25 m s^{-1}) approach this turbulence-dominated regime, our ballistic residence times in these conditions may understate true residence time and thus underestimate spray CO_2 flux. Large-eddy simulation results for hurricane-force conditions reinforce that droplet lifetime is not well captured by terminal-velocity/wave-height estimates alone (Richter et al., 2025). Transport dimensionality is therefore a distinct source of residence-time uncertainty, independent of the terminal-versus-acceleration question this paper addresses.

Most spray-mediated flux schemes in the broader Andreas-lineage of spray heat/momentum flux algorithms use terminal velocity for droplet fall speed because it is closed-form and computationally cheap. We show that for conditions representative of real developing seas, that assumption introduces bias in modeled spray-driven CO_2 flux. That bias is especially significant at high winds where spray flux approaches the magnitude of interfacial and bubble-mediated exchange (Wanninkhof, 2014; Deike and Melville, 2018). We have found that the formulation of droplet fallspeed affects spray-driven gas flux, suggesting that it may also influence models of heat and moisture fluxes used in hurricane prediction. Future work should quantify the sensitivity of these fluxes to fallspeed formulation across a range of wind and sea-state conditions. Although more physically realistic fallspeed formulations increase computational cost, this sensitivity analysis will help determine whether the resulting improvements in accuracy justify that additional expense or whether the computationally efficient terminal-velocity approximation is sufficient.

Code and data availability

Code and data associated with the model and model results are published in the Zenodo repository (Hendrickson et al., 2026) and are available at the following DOI: https://doi.org/10.5281/zenodo.23068190

Author contributions

LR and LH designed the study. LH conducted the modelling and data analyses and wrote the manuscript. LR and PV read the manuscript and provided comments and edits.

Competing interests

The contact author has declared that none of the authors has any competing interests.

Acknowledgements

Funding for this project was provided by NSF grant no. 2218781 to Penny Vlahos, Leonel Romero, and Lucy Hendrickson.

https://doi.org/10.5194/egusphere-2026-6668
Preprint. Discussion started: 12 November 2026
© Author(s) 2026. CC BY 4.0 License.

Financial support

This research has been supported by the National Science Foundation grant no. 2218781.

References

Andreas, E. L.: Time constants for the evolution of sea spray droplets, Tellus B, 42, 481–497, https://doi.org/10.1034/j.1600-0889.1990.t01-3-00007.x, 1990.

Andreas, E. L.: Sea spray and the turbulent air–sea heat fluxes, J. Geophys. Res.-Oceans, 97, 11429–11441, https://doi.org/10.1029/92JC00876, 1992.

Andreas, E. L., Vlahos, P., and Monahan, E. C.: Spray-mediated air–sea gas exchange: the governing time scales, J. Mar. Sci. Eng., 5, 60, https://doi.org/10.3390/jmse5040060, 2017.

Angle, K. J., Crocker, D. R., Simpson, R. M. C., Mayer, K. J., Garofalo, L. A., Moore, A. N., Mora Garcia, S. L., Or, V. W., Srinivasan, S., Farhan, M., Sauer, J. S., Lee, C., Pothier, M. A., Farmer, D. K., Martz, T. R., Bertram, T. H., Cappa, C. D., Prather, K. A., and Grassian, V. H.: Acidity across the interface from the ocean surface to sea spray aerosol, P. Natl. Acad. Sci. USA, 118, e2018397118, https://doi.org/10.1073/pnas.2018397118, 2021.

Barr, B. W., Chen, S. S., and Fairall, C. W.: Sea-state-dependent sea spray and air–sea heat fluxes in tropical cyclones: a new parameterization for fully coupled atmosphere–wave–ocean models, J. Atmos. Sci., 80, 933–960, https://doi.org/10.1175/JAS-D-22-0126.1, 2023.

Beard, K. V.: Terminal velocity and shape of cloud and precipitation drops aloft, J. Atmos. Sci., 33, 851–864, https://doi.org/10.1175/1520-0469(1976)033<0851:TVASOC>2.0.CO;2, 1976.

Deike, L. and Melville, W. K.: Gas transfer by breaking waves, Geophys. Res. Lett., 45, 10482–10492, https://doi.org/10.1029/2018GL078758, 2018.

Grythe, H., Ström, J., Krejci, R., Quinn, P., and Stohl, A.: A review of sea-spray aerosol source functions using a large global set of sea salt aerosol concentration measurements, Atmos. Chem. Phys., 14, 1277–1297, https://doi.org/10.5194/acp-14-1277-2014, 2014.

Fridlind, A. M. and Jacobson, M. Z.: A study of gas–aerosol equilibrium and aerosol pH in the remote marine boundary layer during the First Aerosol Characterization Experiment (ACE 1), J. Geophys. Res.-Atmos., 105, 17325–17340, https://doi.org/10.1029/2000JD900209, 2000.

Hendrickson, L., Vlahos, P., and Romero, L.: Timescales for the spray-mediated gas exchange of carbon dioxide, J. Mar. Sci. Eng., 12, 1128, https://doi.org/10.3390/jmse12071128, 2024.

Hendrickson, L., Romero, L., and Vlahos, P.: Sea spray driven CO_2 efflux: modeling the effect of sea spray evaporation on carbonate chemistry and air–sea gas exchange, npj Clim. Atmos. Sci., 9, 31, https://doi.org/10.1038/s41612-025-01304-5, 2025.

https://doi.org/10.5194/egusphere-2026-6668
Preprint. Discussion started: 12 November 2026
© Author(s) 2026. CC BY 4.0 License.



Hendrickson, L., Romero, L., and Vlahos, P.: Spray-Mediated CO2 Flux: Sensitivity to Droplet Fall-Speed Formulation, Zenodo [code], https://doi.org/10.5281/zenodo.23068190

Keene, W. C., Sander, R., Pszenny, A., Vogt, R., Crutzen, P. J., and Galloway, J. N.: Aerosol pH in the marine boundary layer: a review and model evaluation, J. Aerosol Sci., 29, 339–356, https://doi.org/10.1016/S0021-8502(97)10011-810011-8), 1998.

Keene, W. C., Pszenny, A. A. P., Maben, J. R., and Sander, R.: Variation of marine aerosol acidity with particle size, Geophys. Res. Lett., 29, 1101, https://doi.org/10.1029/2001GL013881, 2002.

Mueller, J. A. and Veron, F.: Impact of sea spray on air–sea fluxes. Part I: Results from stochastic simulations of sea spray drops over the ocean, J. Phys. Oceanogr., 44, 2817–2834, https://doi.org/10.1175/JPO-D-13-0245.1, 2014.

Pszenny, A. A. P., Moldanová, J., Keene, W. C., Sander, R., Maben, J. R., Martinez, M., Crutzen, P. J., Perner, D., and Prinn, R. G.: Halogen cycling and aerosol pH in the Hawaiian marine boundary layer, Atmos. Chem. Phys., 4, 147–168, https://doi.org/10.5194/acp-4-147-2004, 2004.

Richter, D. H., Bryan, G. H., Dennis, J., Sun, J., and Voelz, S.: Large-eddy simulation of the spray-laden hurricane boundary layer: I. Spray transport and statistics, J. Geophys. Res.-Atmos., 130, e2025JD044054, https://doi.org/10.1029/2025JD044054, 2025.

Romero, L.: Distribution of surface wave breaking fronts, Geophys. Res. Lett., 46, 10463–10474, https://doi.org/10.1029/2019GL083408, 2019.

Staniec, A., Vlahos, P., and Monahan, E. C.: The role of sea spray in atmosphere–ocean gas exchange, Nat. Geosci., 14, 593–598, https://doi.org/10.1038/s41561-021-00796-z, 2021.

van Boxel, J.: Numerical model for the fall speed of raindrops in a rainfall simulator, I.C.E. Special Report 1998/1, https://dare.uva.nl/search?identifier=f900db81-bbe8-43eb-b266-676dbfb7ba6d, 1998.

Voermans, J. J., Babanin, A. V., and Troitskaya, Y.: A note on the settling velocity of sea spray spume droplets, J. Phys. Oceanogr., https://doi.org/10.1175/JPO-D-25-0162.1, 2026.

Wanninkhof, R.: Relationship between wind speed and gas exchange over the ocean revisited, Limnol. Oceanogr.-Meth., 12, 351–362, https://doi.org/10.4319/lom.2014.12.351, 2014.

Weiss, R. F.: Carbon dioxide in water and seawater: the solubility of a non-ideal gas, Mar. Chem., 2, 203–215, https://doi.org/10.1016/0304-4203(74)90015-2, 1974.